Dynamic derailment simulation of an empty wagon passing a turnout in the through route

Dynamic derailment simulation of an empty wagon passing straight through turnout

Xin Ge[1], Liang Ling[1], Lirong Guo[2], Zhiyong Shi[1, 3], Kaiyun Wang[1*]

1. State Key Laboratory of Traction Power, Southwest Jiaotong University, Chengdu, China.

2. Locomotive & Car Research Institute, China Academy of Railway Sciences Corporation Limited, Beijing, China.

3. Department of Industrial Engineering, University of Florence, Florence, Italy

Corresponding author: Kaiyun Wang

E-mail: kywang@swjtu.edu.cn.

Dynamic derailment simulation of an empty wagon passing straight through turnout

Abstract: Turnout is recognized as one of the weakest links of railway lines. Based on the field investigation results in a wheel climb derailment scene, this paper presents a study on the dynamic derailment behavior of an empty wagon passing straight through a turnout. The potential factors that inducing train derailment in turnout area are firstly analyzed, from both the train and track aspects. Then a dynamic wagon-turnout interaction model considering the non-uniform cross-sections of rails and the interaction of adjacent wagons, is developed using the SIMPACK and validated by the field test data. By means of numerical simulation, the characteristics of wheel-rail interaction in turnout area are investigated, and the critical influence factors related to derailment are studied in detail. The results indicate that the growing inclined surface of switch rail, the condition of wheel-rail contact surface, and the lateral component of coupler force are responsible for wheel climb derailment in turnout area. The derailment possibility of empty wagons in turnout area increases with the increasing of coupler force and wheel-rail friction coefficient. The risk of wheel climb derailment increases with the decrease of running speed at low speed range. To enhance the running safety of empty wagons in turnout area, the rail lubrication could be implemented, and the large braking forces should be avoided at low-speed condition.

Key words: Turnout; freight wagon; derailment simulation; coupler force; wheel-rail interaction.

1. Introduction

Turnout is one of the most important equipment in railway lines, and plays a key role in transportation organization. Cross-sections of the switch and the frog rails change

with the increasing distance from the toe of the switch, especially the harmful space in the frog area, which intensifies the wheel-rail interaction and raises the derailment risk of the operating trains [1]. According to the statistics of more than 130 derailments in the UK over the last 15 years, the accidents that happened in turnout areas account for about 35% of the total [2]. In practice, the railway operators pay much attention on the running safety of vehicles running through turnout branch, and neglect the risk of trains passing straight through turnout. During the actual operation of heavy-haul railways, the train operator would take no additional protective measures in locomotive control when the trains cross straight through turnout. However, the derailment accidents have occurred persistently in railway turnouts, which has gradually attracted much attention on the running safety of trains passing straight through turnout. Therefore, it is of great significance to investigate the dynamic derailment behavior of trains passing straight through turnout.

To evaluate the risk of wheel flange climb derailment, Nadal proposed the well-known single-wheel L/V limit criterion in 1896 [3]. The derailment coefficient (the ratio of lateral wheel-rail force to vertical force) is first introduced for assessment of wheel derailment safety. The subsequent field tests and simulations have proved that wheel flange climb derailments would only occur when the L/V ratio limit has been exceeded for a certain distance limit or time duration limit [1]. To perfect the derailment criterion, Weinstock proposed a less conservative wheel flange climb criterion by summing the absolute values of L/V on the two wheels on the same axle, known as the “axle sum L/V” ratio [4]. The criteria based on time duration and wheel

climb distance duration were proposed and adopted by Japanese National Railway (JNR), the Association of American Railroad (AAR) and many other scholars [5-8]. For example, Zhai [9] suggested a 35ms time duration limit for derailment criterion based on derailment coefficient and ratio of wheel unloading. Besides, a new derailment evaluation criterion based on wheel lift was also proposed [10].

The development of computer simulation technology greatly promotes the studies on derailment mechanism. Zeng et al. [11, 12] conducted a series of researches on train derailment based on random energy analysis theory. Barbosa [13] derived an extended three-dimensional formula for the railway wheel flange climb derailment process and simulated the derailment phenomenon of single wheelset. Zeng et al. [14, 15] studied the mechanism of wheel flange climb derailment based on theoretical analysis and a single-wheelset test rig. It is revealed that the large lateral wheel-rail force and reduced vertical force were responsible for the wheel climb derailment. Ling et al. [16] investigated the dynamic behavior and derailment mechanisms of trains under lateral impact based on a fully nonlinear three-dimensional dynamic model.

Focus on specific problems in turnout area, a lot of researches by means of simulation and field test have been carried out. Based on analysis of frequent flange climb derailments in sharp curves or curves within turnout subsequent to wheel turning, the condition of the turned wheel surface is supposed to be responsible. By means of experiments and numerical simulations, the relationship between the running safety of vehicles and its surface condition was investigated, and the

lubrication just after turning is proposed to reduce flange climb derailment [17]. Xu et al. [18] established an elasticity positioning wheelset model based on a coupled finite element method and multi-body dynamics and studied the dynamic wheel–rail interaction during a wheel flange climbs on the turnout rails. Besides, the influence of rail wear on wheel-rail interaction in turnout area was investigated in Ref. [19]. Sun et al. [20] simulated the wheel impact forces due to the interaction between vehicle and a turnout in VAMPIRE environment. Dos et al. [21] modelled the wagons and the characteristics of the track geometry using NUCARS. The influences of side bearing clearance and wheel profile on vehicle dynamic behaviors were simulated, and the field test data was employed to validate it. Ren [22, 23] developed a comprehensive vehicle/turnout system coupling dynamic model considering wheel-rail multi-point contacts and studied the characteristic of vehicle-turnout system. Kassa et al. [24] conducted field tests on dynamic interaction between train and railway turnout and established a dynamic train-turnout interaction model in GENSYS environment. The influences of train speed and moving direction on the vertical and lateral contact forces were investigated.

The previous research on train derailment in turnout area mainly based on a single wheelset (or vehicle) model without considering the interaction between the adjacent vehicles of a long heavy-haul train. The longitudinal coupler forces are proved to have great influence on the derailment of vehicles [25-28]. Based on the field investigation of a derailment accident in turnout area, this paper presents a detailed dynamic derailment simulation of an empty wagon passing straight through a

turnout. Firstly, the potential risks of wheel-rail interaction in turnout area are analyzed based on the field investigation result. Secondly, a detailed dynamic model of wagon-turnout interaction is established by considering the non-uniform cross-sections of rails and longitudinal interaction of adjacent wagons, and the field test data is employed to validate this model. Then, the characteristic of wheel-rail interaction in turnout area is investigated based on the model. Finally, the influences of coupler force, wheel-rail friction coefficient as well as running speed on the derailment of an empty wagon in turnout area are studied. This study could provide theoretical guidance for enhancing the running safety of heavy-haul trains in turnout.

2 Potential factors inducing train derailment in turnout area

According to the field investigation results, this section presents a deep analysis on the potential factors that inducing train derailment in turnout area from track system and train system aspects.

2.1 The track system

Differing from the main track rails, the cross-sections of the rails in turnout area change in the longitudinal direction from the toe of switch. Figure 1 shows the configuration of a typical heavy-haul turnout. The turnout is mainly composed of a switch rail and a fixed frog. The top width and height of the switch rails gradually increase from the switch blade towards the frog as shown in figure 1 (a). It can be seen in Figure 1 (b), there exists harmful space (discontinuity of rail cross-sections) at the transition area between the tongue rail and the through rail. The non-uniform

cross-sections of rail produce an intrinsic track irregularity, which intensify the wheel-rail interaction. Figure 2 shows the typical geometrical contact between wheel and rail in turnout area. Both the contact points on the stock rail and the switch rail (or on the wing rail and the through rail) have a narrow distribution. Due to the large gap between the concentrated contact areas, the contact points will jump under the effect of large lateral wheelset force. Besides, the transition between the stock rail and switch rail (or between the tongue rail and the through rail) will cause the jump of contact points either, which will lead to severe wheel-rail impact vibrations. Furthermore, the initial top heights of switch rail and through rail are low. The growing cross-sections produce a gentle inclined surface in longitudinal direction. Under the effect of large lateral force, the wheel flange approaches the rail, and the wheel is more likely to climb onto the rail top.

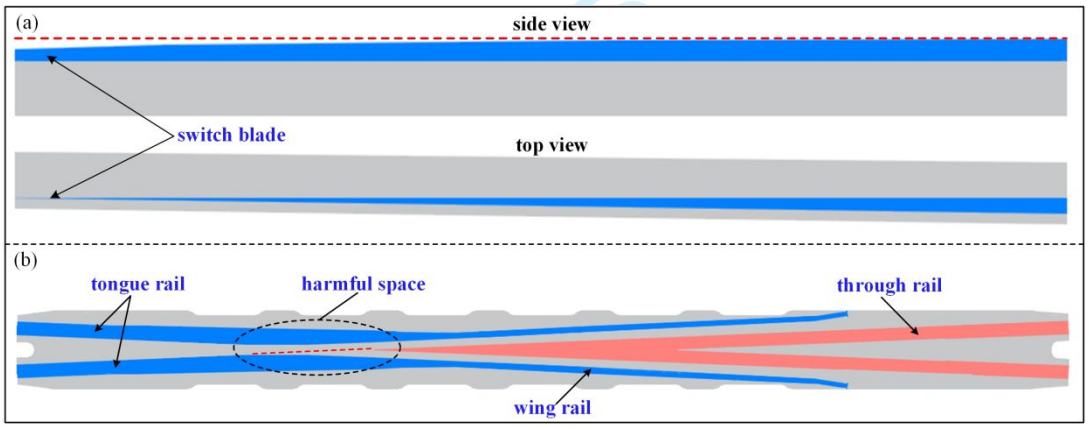

Figure 1. The structure scheme of a typical heavy-haul turnout: (a) the switch rail; (b) the fixed frog.

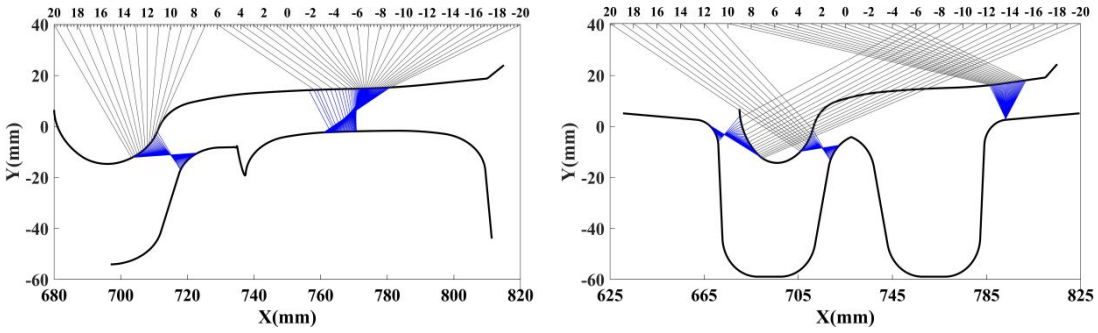

(a) (b)

Figure 2. Typical geometrical contact between wheel and rail in turnout area: (a) switch rail with top width of 20mm, (b) frog rail with top width of 20mm.

2.2 The train system

Comparing to the track system, the situation of the train system is more complicated. The performance degradation of key components, the interaction of adjacent wagons (or locomotives) as well as the loads and train speed have significant effects on the train running safety.

It can be seen in Figure 3 (a) that the employed K6-type bogie is a typical three-piece bogie with a simple suspension system. The primary suspensions adopt the rubber blankets mounted on the adapters. The secondary suspensions are composed of coil groups with two-stage stiffness and wedge friction dampers. Besides, a cross-sustaining device is equipped to enhance the diamond-resistant rigidity and hunting stability. The vibration energy of the wagon system is mainly dissipated by means of frictional resistance provided by wedge friction dampers. Due to the wear of long-term service, the damping performance of the wedge friction damper will degrade rapidly, which affects the dynamic performance of wagons significantly. Moreover, the condition of wheel-rail contact surface has a decisive influence on the

running safety of trains. Figure 3 (b) shows the wheel tread and flange of a derailed wagon. It is seen that the cutting traces of re-profiling are still obvious after a period of service, which is an abnormal phenomenon for an in-service wagon. The rough wheel surface will increase the wheel-rail friction coefficient and contribute to the wheel climb [17]. The evident wear marks in flange area indicates the intensive flange-rail interaction during the wheel climbing. Figure 3 (c) exhibits the conditions of coupler shank and coupler yoke of the accidental wagon. Since the maximum dynamic braking force of the accidental train is around 800kN, which is much less than the permitted coupler force, it is reasonable to speculate that the intensive lateral interaction between the coupler shank and coupler yoke during derailment caused the fracture of the coupler shank. The free yaw angle of this type of coupler is 13 degrees. The field test results indicate that the maximal coupler yaw angles of the empty wagons are usually no more than 4 degrees under normal operating conditions. With a comprehensive consideration of the severe wear in flange area in Figure 3 (b) and wheel moving trace on switch rail in Figure 3 (d), it is deduced that an original yaw angle led to a large lateral component of coupler force, which made the wheel flange approach the rail. Under the effect of continuous large lateral force, the wheel climbed onto the rail top along the growing switch rail, and the coupler yaw angle further increased to the limited angle. The violent collisions between coupler shank and coupler yoke happened during the post-derailment process, which caused the cracks on the coupler yoke and the fracture of coupler shank eventually. The coupler force and the coupler yaw angle are speculated as the critical influence factors to the

running safety of the empty wagons. Moreover, the loads and running speed affect the running safety of the wagon as well. In comparison to the fully loaded wagon, the empty wagon has higher wheel unloading rates and derailment coefficients when the same external excitation is applied, and the empty wagons require less lateral force for wheel climb derailment. The running speed influences the wheel-rail contact state remarkably and further affects the wheel-rail interaction.

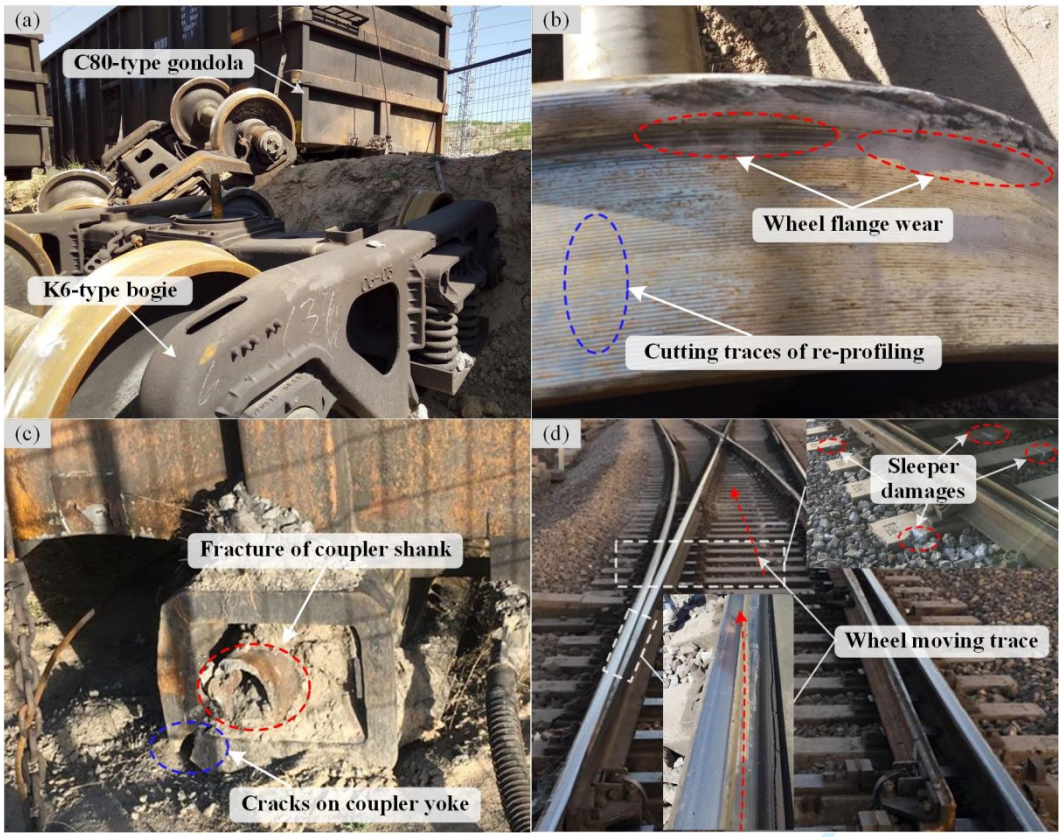

Figure 3. Damaged components in a derailment scene: (a) the accidental wagons, (b) wheel tread and flange, (c) coupling devices and (d) the turnout structure.

3. Wagon-turnout interaction model

To simulate the dynamic behavior of empty wagons in turnout area, a wagon-turnout interaction model was established using SIMPACK, as shown in Figure 4. The model

is mainly composed of two wagons, two drawbar-buffer systems, one dummy wagon and a railway turnout system. A force with initial yaw angle is applied on the car body of the front wagon (the wagon No. 1) to simulate the coupler force.

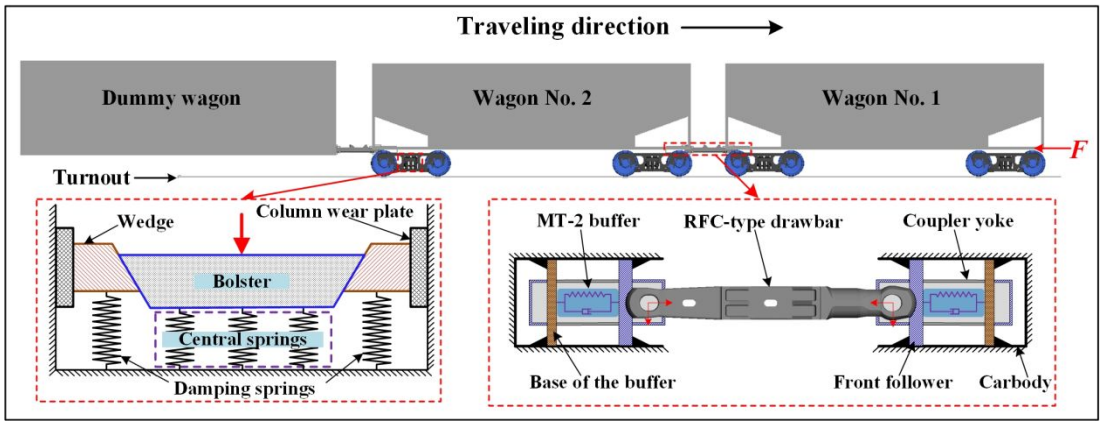

Figure 4. Wagon-turnout interaction model.

3.1 Wagon model

A single wagon model is composed of a car body, two K6-type bogies, and has 74 degree of freedoms (DOFs) in total. The Chinese LM-type wheels are adopted. Each car body, the side frame and the wheel set have 6 DOFs. The adapter is mounted on the axle with only one rotation DOF about Y-axis. The enlarged view in lower-left corner of Figure 4 shows the wedge suspension system model. The column wear plate is treated as part of the side frame. The bolster has two DOFs to move vertically and to yaw, and the wedge has one DOF to move vertically. The dummy wagon has only one DOF to move longitudinally. The interaction of sliding surfaces (such as the side bearings, the center plates, the bolsters, the wedges and the column wear plate) are modelled with Coulomb friction law.

$$F_{\mathrm{f}}=\begin{cases}0 & |v_{\mathrm{T}}|=0\\ \dfrac{|v_{\mathrm{T}}|}{v_{\mathrm{eps}}}\cdot\mu_0\cdot F_{\mathrm{N}}\cdot\mathrm{sign}(v_{\mathrm{T}}) & |v_{\mathrm{T}}|\le v_{\mathrm{eps}}\\ \mu_0\cdot F_{\mathrm{N}}\cdot\mathrm{sign}(v_{\mathrm{T}}) & |v_{\mathrm{T}}|>v_{\mathrm{eps}}\end{cases} \quad (1)$$

where μ_0 is the friction coefficient between the contact surfaces; F_{N} is the normal contact force; v_{T} is the relative tangential velocity; v_{eps} is the limit velocity between regularized friction and slipping Coulomb friction. The main parameters of a wagon are listed in Table 1.

Table 1. Main parameters of C80-type wagon.

Item		Value	Unit
Axle load		25000	kg
Mass of car body (empty/loaded)		10297/90297	kg
Mass of bogie		4800	kg
Mass of wheelset		1171	kg
Wheelbase		1.83	m
Bogie distance		8.2	m
Wheelset radius		0.42	m
Length over pulling faces of couplers		12	m
Primary suspension stiffness (empty/loaded)	Longitudinal	13	MN/m
	Lateral	11	MN/m
	vertical	160	MN/m
Secondary suspension stiffness (empty/loaded)	Longitudinal	1.818/3.127	MN/m
	Lateral	1.818/3.127	MN/m
	vertical	2.233/4.235	MN/m
Axial stiffness of the cross-sustaining device		14.8	MN/m
Pre-pressure of side bearings		19.8	kN

3.2 Inter-vehicle connection model

The enlarged view in the lower-right corner of Figure 4 shows the model of RFC/MT-2 drawbar/buffer system. The system consists of a RFC-type drawbar, coupler yokes, front followers and buffers. The drawbar has four DOFs, including rotation DOFs about X-, Y- and Z-axis as well as linear movement along X-axis. The front follower has one DOF to move longitudinally. The coupler yoke is modelled as a nonlinear torsional spring. The restoring moment Tr is described as [27]:

$$T_{\mathrm{r}}=\begin{cases}0 & |\alpha|<\alpha_{\mathrm{free}}\\ l\left[\alpha-\alpha_{\mathrm{free}}\cdot\mathrm{sign}\left(\alpha\right)\right]\cdot K_{\mathrm{tr}} & |\alpha|\geq\alpha_{\mathrm{free}}\end{cases} \tag{2}$$

where α is the rotation angle; α_{free} is the maximal free rotation angle; l is the distance between the two pin holes of the drawbar; K_{tr} is the angular stiffness of the torsional spring, which has a value of 10^8N/rad. The interaction between the drawbar tail and the follower is modelled as a unilateral contact force in X-axis and rotational friction forces about X-, Y- and Z-axis. The buffer is modelled as a nonlinear spring with hysteresis characteristic, as shown in Figure 5. The buffer impedance force $F_{\mathrm{c}}(x, \Delta v)$ is described as [30, 31]:

$$F_{\mathrm{c}}=\begin{cases}\frac{1}{2}\left[f_{\mathrm{l}}\left(x\right)+f_{\mathrm{u}}\left(x\right)\right]+\frac{1}{2}\left[f_{\mathrm{l}}\left(x\right)-f_{\mathrm{u}}\left(x\right)\right]\cdot\mathrm{sign}\left(\Delta v\right) & |\Delta v|>v_{\mathrm{f}}\\ \frac{1}{2}\left[f_{\mathrm{l}}\left(x\right)+f_{\mathrm{u}}\left(x\right)\right]+\frac{1}{2}\left[f_{\mathrm{l}}\left(x\right)-f_{\mathrm{u}}\left(x\right)\right]\cdot\frac{\Delta v}{v_{\mathrm{f}}}\mathrm{sign}\left(\Delta v\right) & |\Delta v|>v_{\mathrm{f}}\end{cases} \tag{3}$$

where x is the buffer stroke; Δv is the change rate of buffer stroke; v_{f} is the switch speed between the loading and unloading conditions; $f_{\mathrm{l}}(\mathrm{x})$ and $f_{\mathrm{u}}(\mathrm{x})$ represent the loading and unloading forces of the buffer, respectively.

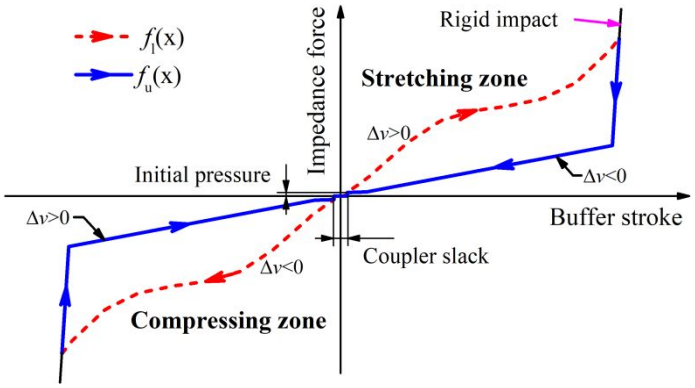

Figure 5. The nonlinear hysteresis of the buffer.

3.3 Turnout model

The employed turnout in this paper is the Chinese No. 12 turnout specially designed for heavy haul railway, as shown in Figure 6. The turnout length is about 35m, while the switch length is 14.211m and the frog length is 5.992m. The permissible maximum passing speed of this type of turnout is 90km/h. To model the variable rail profiles along the track, the rail cross sections are extracted from the CAD drawings. To enhance the smooth transition of adjacent profiles, the profiles are provided about every centimeter along the track, and the variable profiles between the various profiles in longitudinal direction are interpolated by Bézier curves. The sub-graphs (1) ~ (3) in Figure 6 show the variable rail profiles of switch, check rail and frog area, respectively. It should be noted that only the potential contact areas of rails are taken into account when modelling the turnout. Furthermore, the stock rail is neglected when the switch rail grows to a rail with full width.

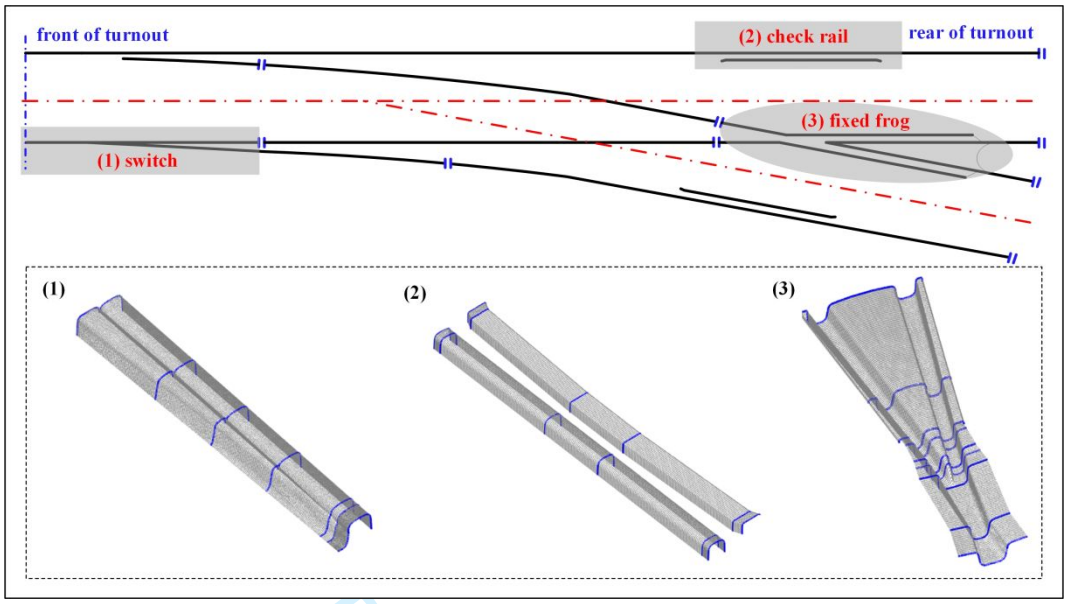

Figure 6. Model of the Chinese No. 12 heavy-haul railway turnout.

3.4 Wheel-rail contact model

A multiple-point contact model is employed to model the complex wheel-rail contact relationship. The normal force is calculated by a penetration method based on the Hertzian nonlinear elastic contact theory, which allows a realistic simulation of wheel lift and regain of contact [32]. The tangential force is calculated using the FASTSIM algorithm [33].

3.5 Model validation

To validate the simulation model, the field test results were employed to compare with the simulation results. The test train consists of 2 double-unit SS4-type locomotives and 108 empty C80-type gondolas. The first wagon following the locomotives was selected as the test wagon. The displacement sensors were installed on the side frame to measure the dynamic relative displacements between the side frame and the car body, as shown in Figure 7. The test train passed straight through a

turnout at a speed of 40km/h under coasting condition. Figure 7 (a) and (b) show the comparisons of the simulation and test results of the vertical and lateral relative displacement, respectively. It can be seen that the overall tendency of vertical and lateral displacement obtained by simulation accords with the test results. Both the vertical and lateral displacements increased sharply at the frog area. The vertical displacements fluctuated within 4mm, and the maximum lateral displacement was about 2mm. As the actual rail wear of the test turnout is complicated, the differences between the simulation and the test results are inevitable. Based on the above analysis, the proposed model can simulate the dynamic behavior of the wagon passing the turnout reasonably.

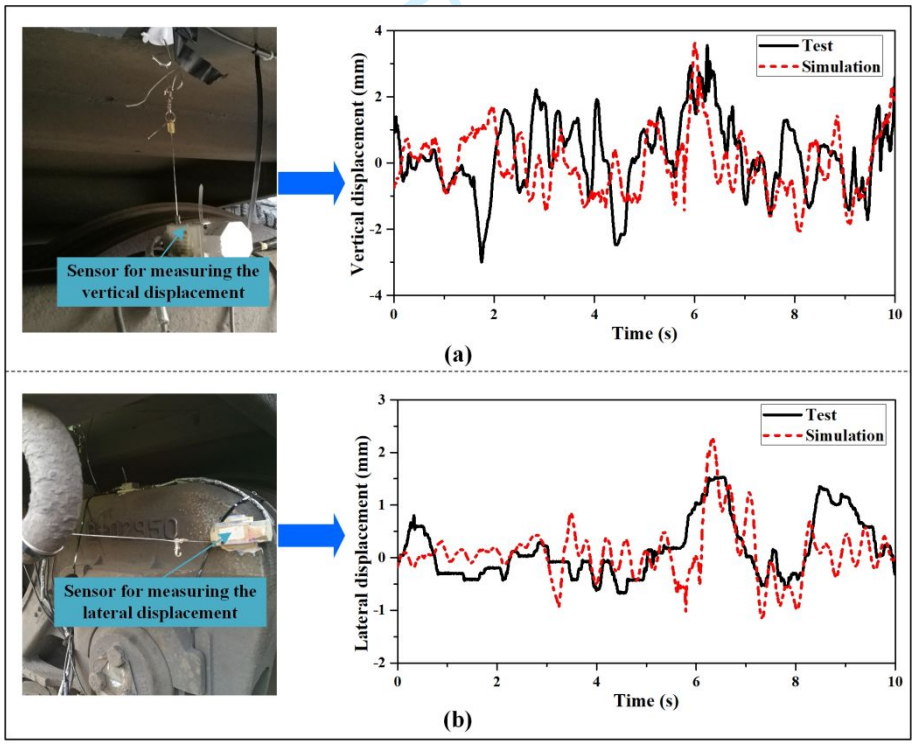

Figure 7. Comparison of tested and simulated results: (a) vertical and (b) lateral relative displacements between the side frame and car body.

4 Characteristics of wheel-rail interaction in turnout area

Based on the validated simulation model reported in Section3, the dynamic behavior of an empty wagon under coasting condition was simulated. As the maximum speed of the empty wagon is usually controlled below 80km/h in realistic operation, the simulation speeds were set as 80km/h. According to the simulation results, the distribution of wheel/rail contact points in turnout area is presented. Moreover, the locations of wheel-rail impact areas are determined, and the characteristics of wheel-rail interaction is discussed in this section.

Figure 8 shows the distribution of contact points on wheel and rail profiles. It is seen that the jumps of contact points occur at x = 3m, 4.75m, 14.05m, 29.75m, 31.5m and 34.6m, respectively. The jumps are caused by the change of the rail profiles when the wheel-rail contact points transit from stock rail to switch rail at about x = 3m and transit from wing rail to through rail at about x = 31.5m. Moreover, the wheel-rail separations happen at around x = 30m, 31.5m and 34.6m.

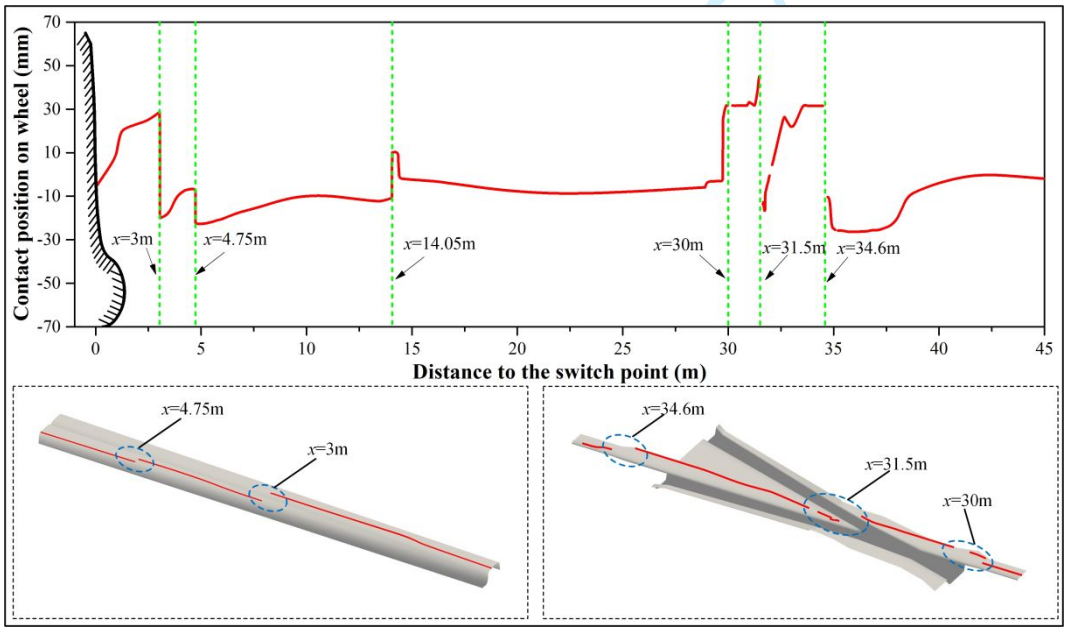

Figure 8. The distribution of contact points on wheel and rail profiles in turnout area.

Figures 9 (a) and (b) show the vertical and lateral wheel-rail forces in time domain, respectively. It is seen that the wheel-rail interaction is gentle in switch area. The vertical and lateral wheel-rail forces fluctuate slightly when the wheel transfers from stock rail to switch rail. The maximal vertical wheel-rail force is about 32kN, and the lateral wheel-rail force is within 4kN. As the wheel travels into the frog area, the wheel-rail interaction is much fiercer than that in switch area. There exist three main wheel-rail impact areas located at front of the frog, the frog nose tip around and the rear of the frog, respectively, which are consistent with three change areas of rail profiles. Among which, the wheel-rail impact about 0.5m behind the frog nose tip is most severe, and the wheel rail instantaneous separation occurs several times, where the wheel transfers from wing rail to the through rail. The maximum vertical wheel-rail force attains 96.88kN, which is almost 4 times of the quasi-static level (about 25kN). The maximum lateral wheel-rail force is about 11kN. The duration of wheel-rail separation is within 15ms. Figures 9 (c) and (d) show the wheel lift and lateral wheelset displacement in time domain, respectively. The wheel lift changes a lot in switch and frog areas, and the range of the wheel lift is within -2 to 2 mm. It is seen that the change rate of wheel lift in frog area is apparently larger than that in switch area, which is consistent with the severer wheel-rail interaction in frog area. The non-uniform cross-sections of rail provoke the hunting motion with long wavelength of the wheelset. The lateral wheelset displacement changes steady along the track, and the maximum lateral wheelset displacement is about 8mm.

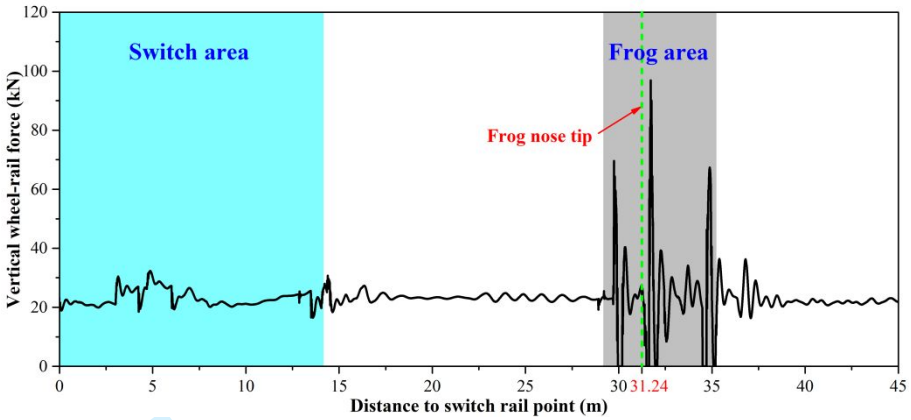
Switch area
Frog area
Frog nose tip
Vertical wheel-rail force (kN)
Distance to switch rail point (m)
31.24

(a)

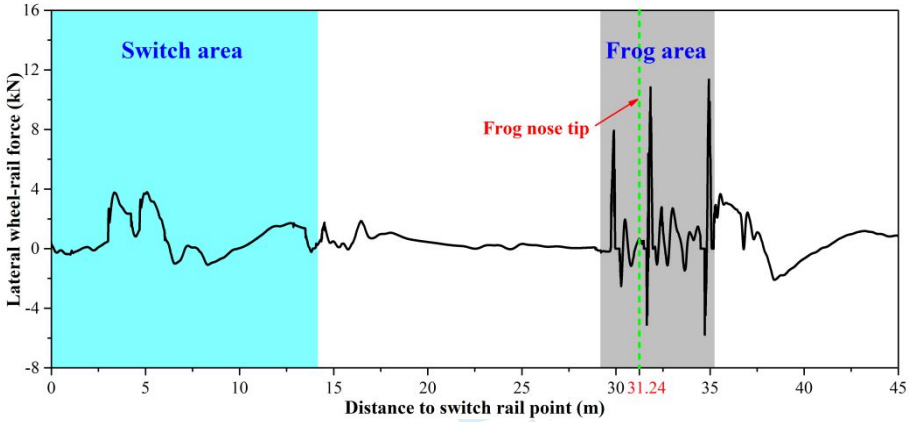
Switch area
Frog area
Frog nose tip
Lateral wheel-rail force (kN)
Distance to switch rail point (m)
31.24

(b)

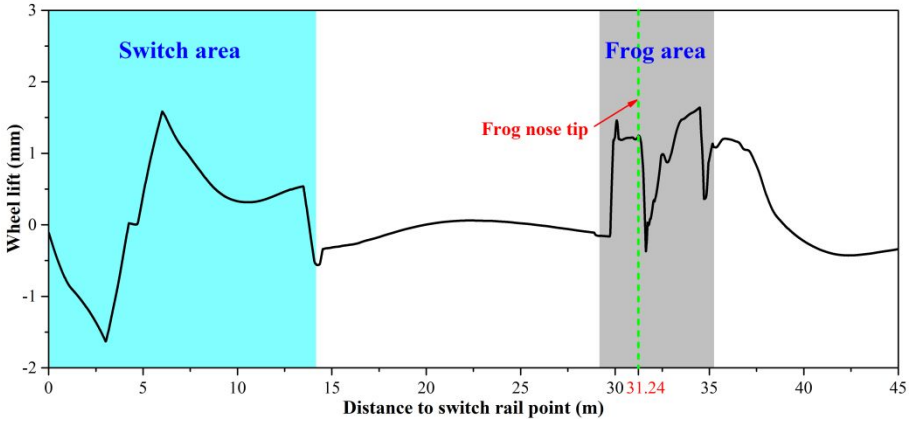
Switch area
Frog area
Frog nose tip
Wheel lift (mm)
Distance to switch rail point (m)
31.24

(c)

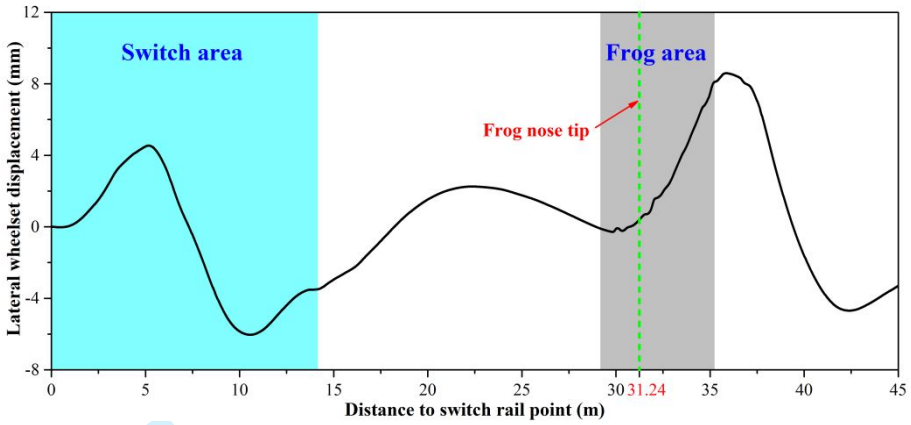

(d)

Figure 9. Dynamic wheel-rail interaction of an empty wagon in turnout under coasting condition: (a) vertical wheel-rail force, (b) lateral wheel-rail force, (c) wheel lift, and (d) lateral wheelset displacement.

5 Dynamic derailment simulation of empty wagons in turnout area

Focusing on the derailment of an empty wagon passing a straight through turnout, the influences of several critical factors on the wheel climb derailment behavior are studied in this section. According to the analysis in the second section, the lateral coupler force, the wheel-rail friction coefficient as well as the train running speed are chosen for further analysis. The lateral coupler force is determined by coupler yaw angle and longitudinal coupler force. To simplify the analysis process, the coupler yaw angle is set to be constant in simulation. The limit value of coupler yaw angle for locomotives is 6 degrees in Chinese railway while the limit value for wagons is not specified. Since the maximum coupler force appears at the first coupler behind the locomotive during dynamic braking while the coupler of wagon is connected to the coupler of locomotive, the coupler yaw angle is fixed as 6 degrees in the simulation

model. Furthermore, the wheel climb derailment generally happens in low-speed range, and the length of the turnout is short, thus the speed of the train can be assumed to be constant. It should be noted that the random track irregularity is not applied in the simulations due to its effect is limited at the turnout zone.

5.1 Derailment critical state

To further analyze the influences of the critical factors on wheel climb derailment, the derailment critical state is determined by simulation. The experimental study conducted by Japanese researchers indicates that the wheel-rail friction coefficient is about 0.3~0.5 under the condition of low velocity and dry environment [34]. The running speed was set to be 40km/h and the friction coefficient was set to be 0.35 during critical state analysis. According to a large number of simulations, when the coupler force attains 696kN (its lateral component is 72.75kN), the wheel climbs onto the switch rail top and drops off the rail soon. When the coupler force is 695kN (the lateral component is about 72.65kN), the wheel climb does not happen. Thus, the derailment critical coupler force can be determined as 696kN.

The distributions of wheel-rail contact points under critical states are shown in Figures 10 (a) and (b), respectively. Under the effect of continuous lateral force originating from coupler force, the wheel flange contacts with the switch rail since the initial position. The distributions of contact points under safe and derailment critical state do not differ a lot at the front of the switch rail. The bifurcation point locates at the position about 3m from the switch rail point, where the width of the switch rail is about 35mm and top of the switch rail is about 3mm lower than that of stock rail.

With the further movement of the wagons, the wheel under derailment critical state climbs up along the growing switch rail and reaches the rail top at the position about 5.5m from the switch rail point. The wheel continues to move forward on the rail head about 1m before dropping off the rail. For the safety critical state, the distributions of wheel-rail contact points keep steady, and the wheel gradually transits to the rail with full width.

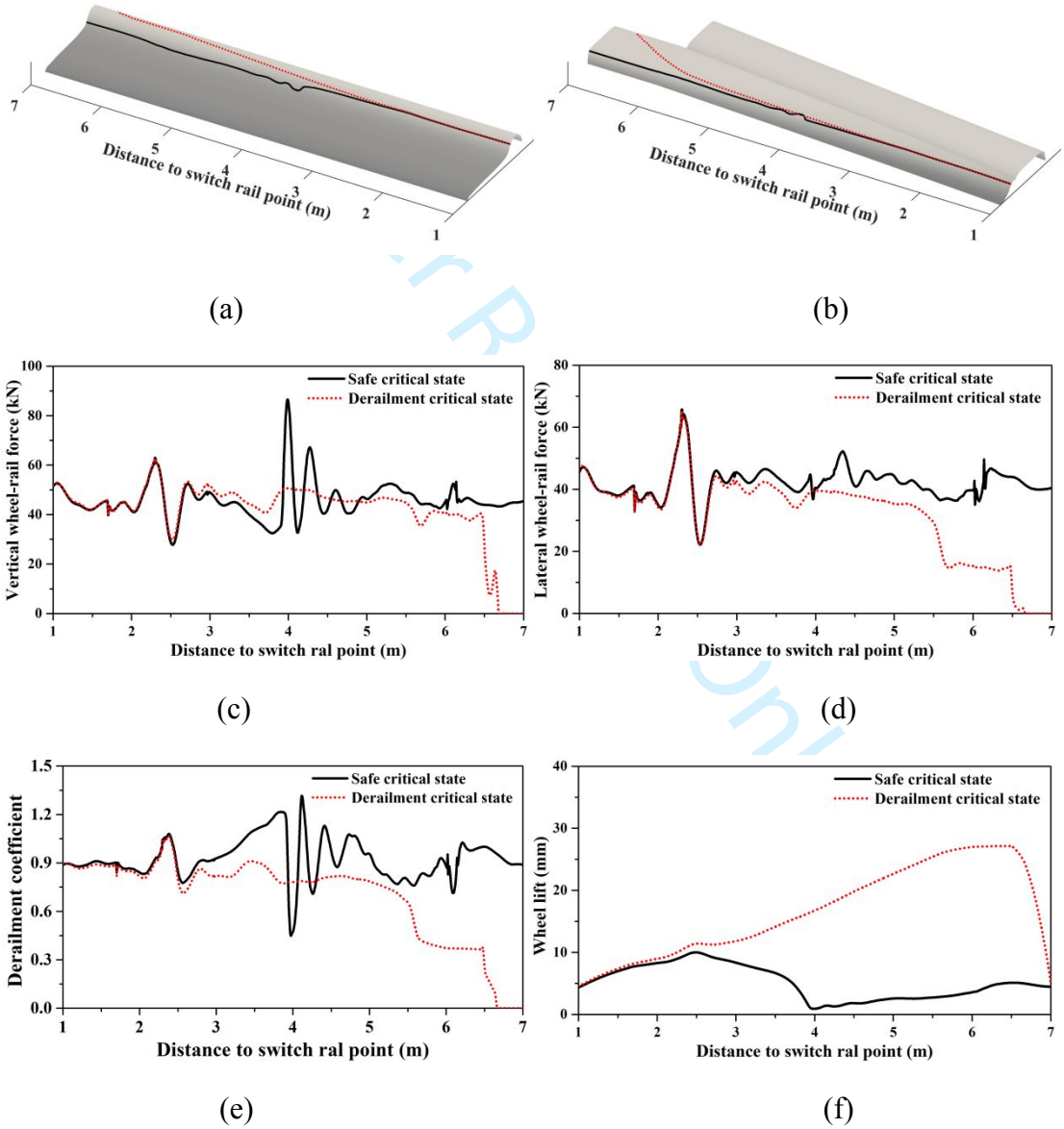

Figure 10. Comparison of dynamic interactions under safe and derailment critical states: (a) distribution of wheel contact points and (b) distribution of rail contact

points, (c) vertical wheel-rail force, (d) lateral wheel-rail force, (e) derailment coefficient and (f) wheel lift.

Figures 10 (c) ~ (f) show the comparison of dynamic wheel-rail interactions under safe and derailment critical states. When the distances of the wheels to the switch rail point are less than 3m, the difference of the wheel-rail dynamic interaction between the safe and derailment critical states is small. As the wheels move forward, the difference becomes more pronounced. For the safe critical state, the vertical wheel-rail force fluctuates sharply affected by the changing cross section of rail while the lateral wheel-rail force changes in a narrow range, and the derailment coefficient fluctuates a lot accordingly. The maximum vertical wheel-rail force attains 86.50kN, and the maximum derailment coefficient exceeds 1.3. For the derailment critical state, both the vertical and lateral wheel-rail forces keep steady during the climbing phase. Similarly, the derailment coefficient does not change a lot. At the position about 5.5m from the switch rail point, the lateral wheel-rail force decreases abruptly from about 34kN to 15kN and stays for a distance, while the vertical wheel-rail force still keeps steady. When the wheel moves to the position about 6.5m away from the switch rail point, the vertical wheel-rail force drops sharply from about 40kN to 8kN, and then raises a little before decreasing to zeros. The lateral wheel-rail force and derailment coefficient decrease to zero till the wheel drops off the rail. It can be seen in Figure 10 (f) that the wheel lift increases gradually to about 27mm first and then drops sharply under derailment critical state. For the safe critical state, the wheel lift increases to about 10mm at the position around 2.5m from switch rail point, and then decreases to a low level.

5.2 Effect of Coupler force

According to the above analysis, the coupler force under derailment critical state is 696kN. Moreover, the maximum dynamic braking force of the locomotives is about 800kN. To further analyze the influences of coupler force on wheel climb derailment, the coupler force was set to be 700, 750 and 800kN while the wheel-rail friction coefficient was set to be 0.35 and the running speed was set to be 40km/h.

It is observed in Figure 11 (a) that the contact points on wheel surface are concentrated in flange area, and the lateral distance between the contact point and the running circle increases with the increasing coupler force. The distributions of contact points on rail head in Figure 11 (b) indicate that the wheel climb is more likely to happen under the cases of large coupler forces. The larger the coupler force is applied, the earlier the derailment happens. Moreover, the wheel will separate from the rail for a short time when the contact point transits from the switch rail to the stock rail, and the transition position moves towards the switch rail point with the increasing coupler force. It can be seen in Figures 11 (a) and (b) that the lateral wheel-rail forces start to gradually decrease as the wheels move on the switch rail top, while the vertical wheel-rail forces still keep steady for a short distance. When the wheels move across the highest point of the rail, the vertical wheel-rail forces begin to decrease. Besides, the re-contact of wheel-rail after instantaneous separation will cause severe wheel-rail impacts. It can be seen that both the maximum vertical and lateral wheel-rail forces decrease as the coupler forces increase. It is shown in Figure 11 (d) that although the wheel lifts increase with increasing coupler forces, the heights of wheel-rail

separations increase with the increasing distances from the separation locations to the switch rail point. This can explain the change law of wheel-rail impact force with coupler force. The overall tendency of derailment coefficient is basically in accord with that of wheel-rail force, as shown in Figure 11 (e).

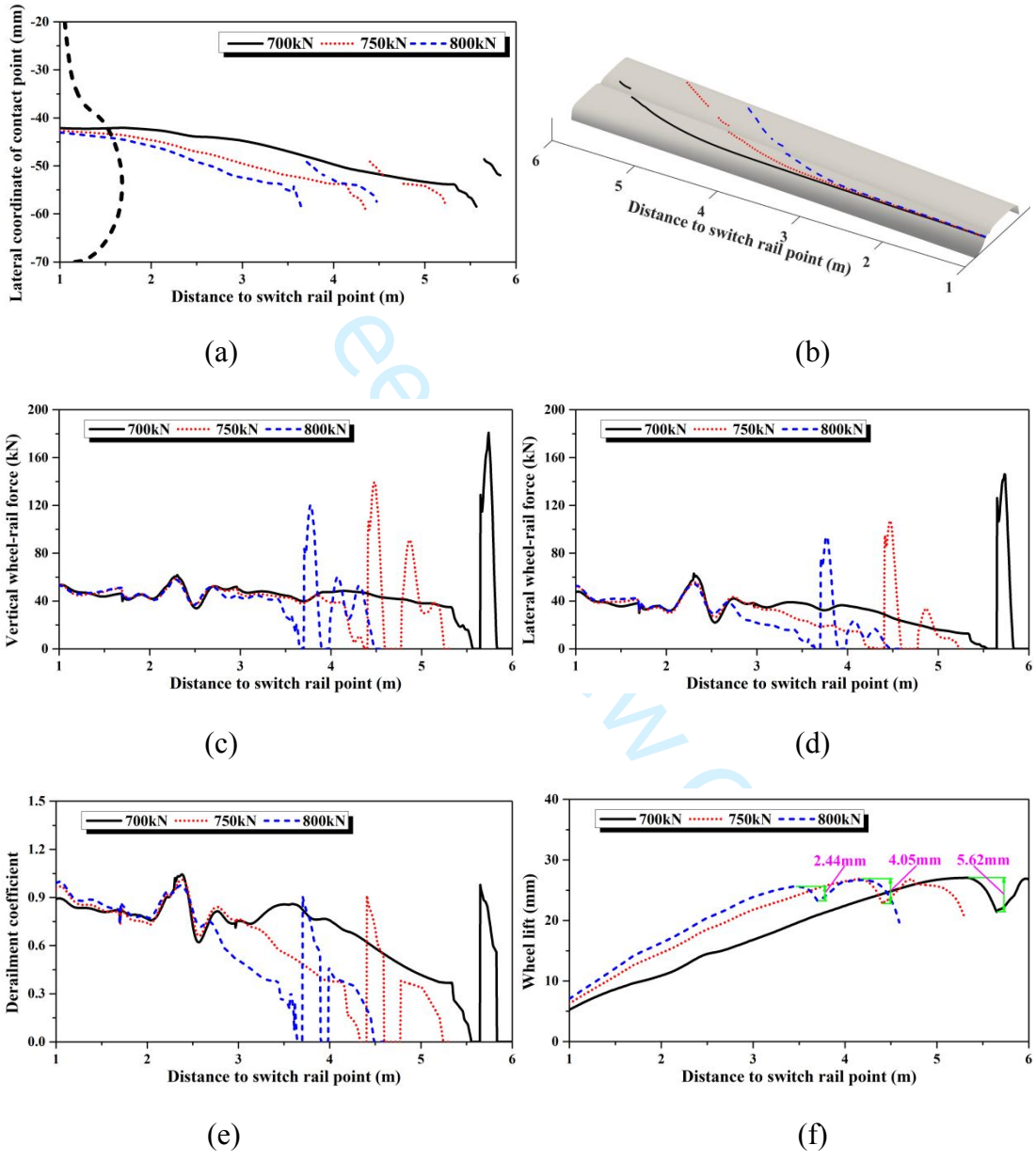

Figure 11. Comparison of dynamic interactions under the effect of different coupler forces: (a) distribution of wheel contact points and (b) distribution of rail contact points, (c) vertical wheel-rail force, (d) lateral wheel-rail force, (e) derailment coefficient and (f) wheel lift.

According to the above analysis, it can be concluded that the large lateral coupler force promotes the wheel climb derailment significantly.

5.3 Effect of Wheel-rail friction coefficient

The wheel-rail friction coefficient is regarded as one of the most important factors for wheel climb derailment. To analyze the influence of wheel-rail friction coefficient on wheel climb derailment, the friction coefficient was set to be 0.2, 0.3, 0.4 and 0.5, the coupler for is set to be 696kN, and the running speed was set to be 40km/h.

Figures 12 (a) and (b) show the distributions of wheel-rail contact points under the conditions of different wheel-rail friction coefficients. It is seen that the contact areas on rail transit from the stock rail to switch rail at the position about 2.3m from the switch rail point when the friction coefficient is 0.2 while the contact areas on wheel transit from the tread to the flange, and the wheel climb does not occur. When the friction coefficient is 0.3, the wheel flange contacts with the switch rail since the initial position. As the wheel moves to the position about 2.25m from the switch rail point, the contact areas move to wheel tread and the stock rail in a short distance, and then return to the wheel flange and switch rail. Similarly, the wheel climb derailment does not appear. When the friction coefficient is increased to 0.4 and 0.5, the wheel flange contacts with the switch rail since the initial position and gradually climbs onto the switch rail top along the growing cross sections under effect of continuous lateral forces. The wheel-rail instantaneous separations happen when the contact points transit from the switch rail to stock rail. Furthermore, the wheel climb derailment happens a little earlier when the friction coefficient is set to be a higher one. When the

wheel moves on the rail top, the friction force between the wheel and rail prevents the further relative movement between the wheel and rail. Therefore, the position of wheel dropping the rail is closer to the switch rail point under the condition of a low wheel-rail friction coefficient.

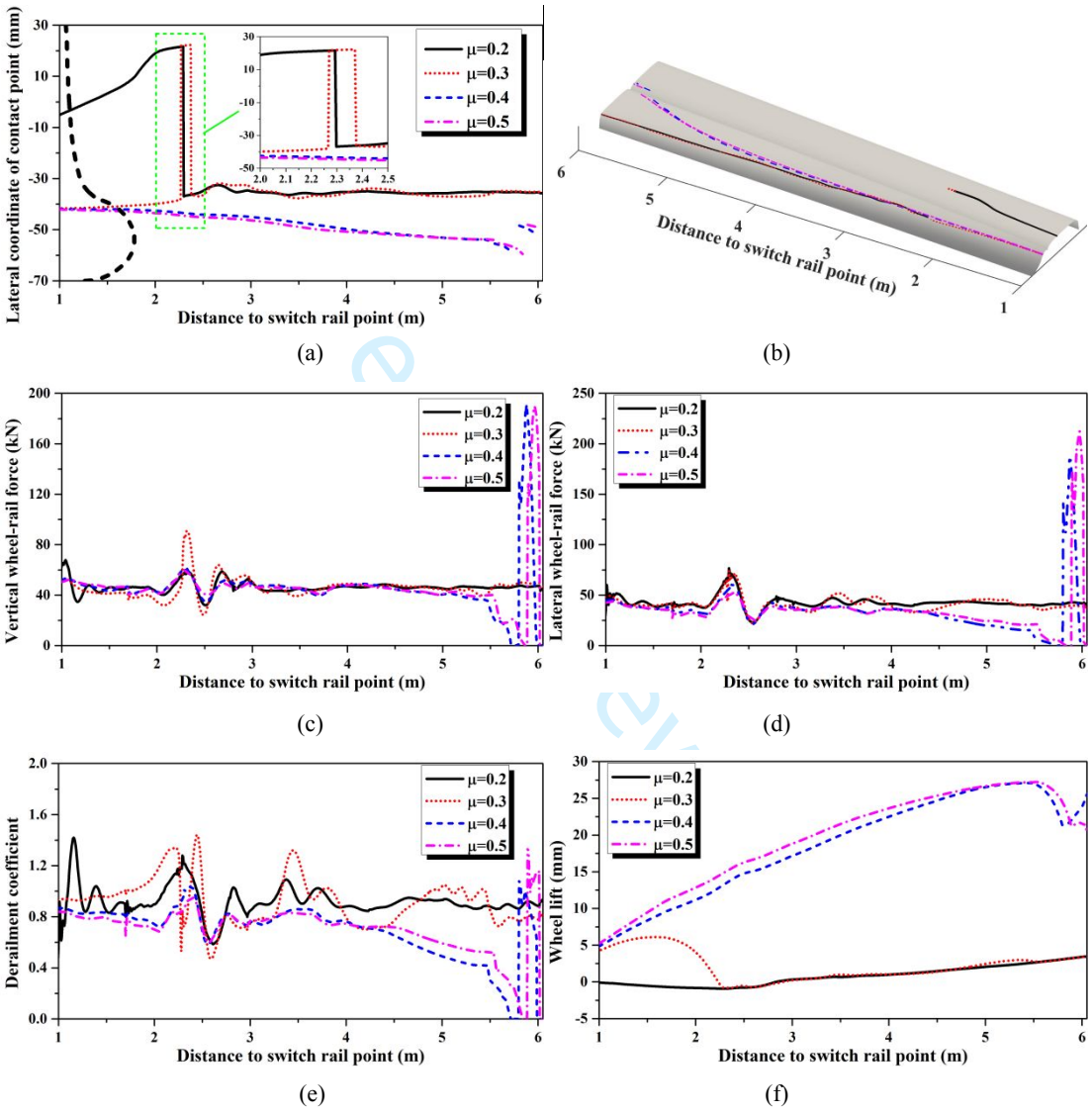

Figure 12. Comparison of dynamic interactions under the condition of different wheel-rail friction coefficients: (a) distribution of wheel contact points and (b) distribution of rail contact points, (c) vertical wheel-rail force, (d) lateral wheel-rail force, (e) derailment coefficient and (f) wheel lift.

Figures 12 (c) ~ (f) show the wheel–rail dynamic interactions under different

friction coefficients. When the friction coefficient is set to be 0.2 and 0.3, both the vertical and lateral wheel-rail forces stay around 50kN, and the derailment coefficients change around 1. The large fluctuations of these indexes only occur at the transition areas of contact points between the switch rail and stock rail. When the friction coefficients are increased to 0.4 and 0.5, the wheel-rail forces keep steady before the wheels climb onto the rail top. Meanwhile, the derailment coefficients fluctuate slightly around 0.8. Since the wheels climb up along the growing switch rail, the lateral wheel-rail forces decrease immediately, and the vertical wheel-rail forces start to decrease only after the wheels move across the highest point of the rail. The wheel-rail forces decrease to zero as the wheels separate with the switch rail. When the wheels contact with the stock rail, the wheel-rail contact surface provokes severe impact. The maximum vertical wheel-rail force attains 190kN while the maximum lateral wheel-rail force exceeds 210kN. Moreover, the vertical forces do not differ a lot, but the lateral force with the friction coefficient of 0.5 is larger than that with the friction coefficient of 0.4. Correspondingly the simulation condition with a higher friction coefficient has a larger derailment coefficient. It can be seen in Figure 12 (d) that the wheel lifts increase significantly with the increasing wheel-rail friction coefficients. Under the condition of friction coefficient of 0.2, the wheel lift is minimal before the wheel contacts with the switch rail. Since the contact points move onto the switch rail, the wheel lift rises slowly with the increasing height of switch rail. When the friction coefficients attain or exceed 0.3, the initial wheel lift is large because the wheels contact with switch rail since the initial position. When the

friction coefficient is 0.3, the wheel lift rises to about 6mm firstly, then descends gradually to the same level of that with friction coefficient of 0.2. Under the conditions of friction coefficients of 0.4 and 0.5, the wheel lifts rise steadily first as the wheels climb onto the switch rail top and then descend gradually since the wheels move across the highest point of the rail. Furthermore, the wheel lift with a smaller friction coefficient descends earlier than that with a larger friction coefficient.

It can be concluded that a low wheel-rail friction coefficient can prevent the wheel climb effectively, and a high friction coefficient can prevent the further movement of the wheel on the rail top as well.

5.4 Effect of running speed

Since the wheel flange derailments generally occur at low-speed condition, the running speed in the simulations was set to be 30km/h, 40km/h and 50km/h for further analysis. The coupler force was set to be 696kN and the wheel-rail friction coefficient was set to be 0.35.

It is seen in Figures 13 (a) and (b) that the distributions of contact points on wheel and rail surfaces change a little and the wheel will not climb onto the rail top when the running speed is 50km/h. As the running speed is decreased to 30km/h or 40km/h, the wheels climb onto the rail top along the growing switch rail and derail soon under the effect of continuous lateral coupler force. Moreover, the wheel climb derailment happens earlier at a lower running speed. Figures 13 (c) and (d) show that the vertical and lateral wheel-rail forces increase with the increasing running speed before the wheel climb. The change of vertical and lateral forces is steady when the

wheels move forward on the rail top. It can be seen in Figure 13 (e) that the intense impact only occurs at the transition area between the switch rail and the stock rail. The derailment coefficient fluctuates a lot under the speed of 50km/h, and the maximum value of it reaches 1.37. When the running speeds are 30km/h and 40km/h, the derailment coefficients keep below 1.1. The wheel lifts increase significantly with the decreasing running speed, as shown in Figure 13 (f). The maximum wheel lift is about 5.6mm under the speed of 50km/h. When the speeds are 30km/h and 40km/h, the wheel lifts increase gradually to about 27mm first and then drop.

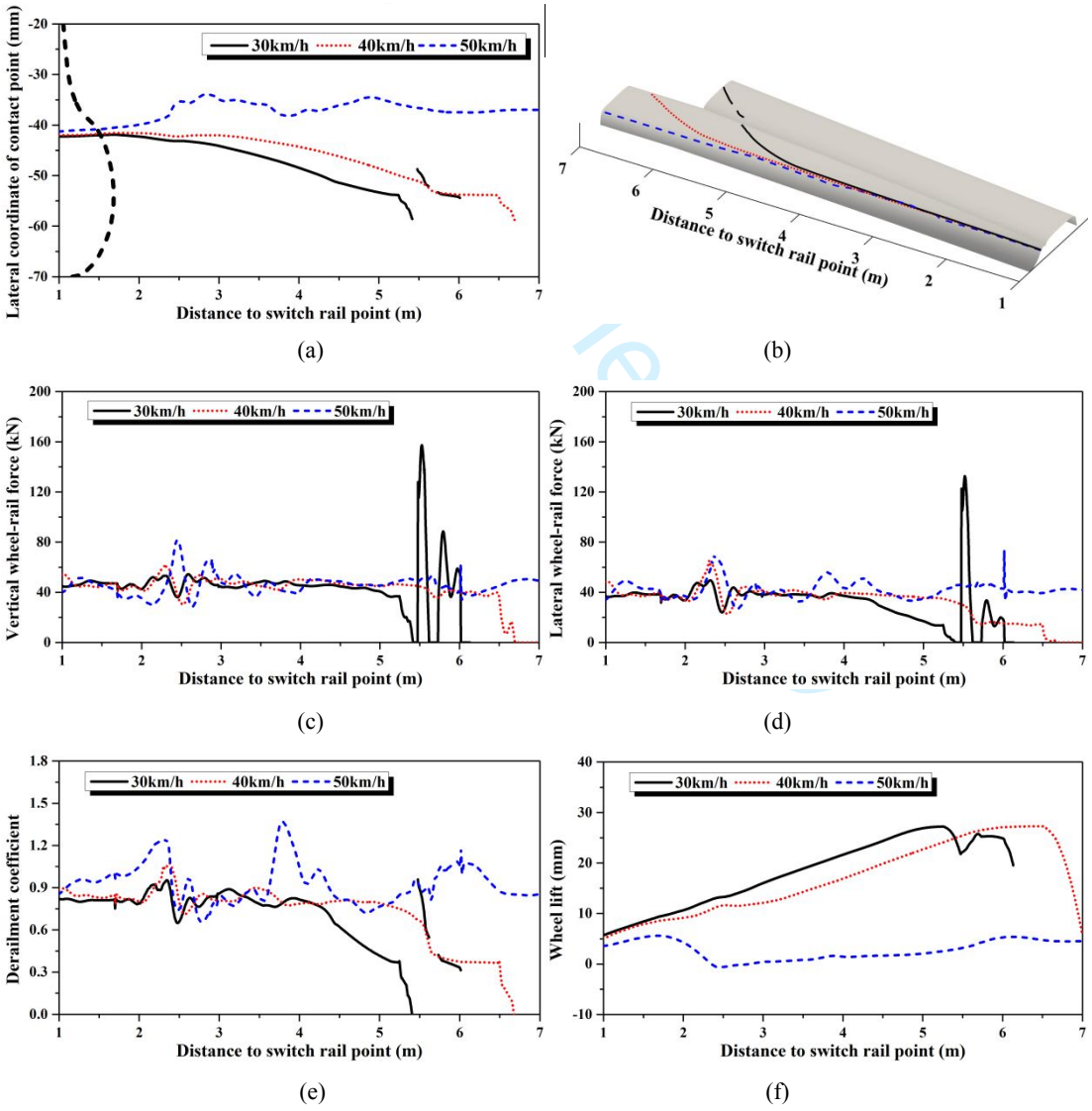

Figure 13. Comparison of dynamic interactions under the condition of different running speeds: (a) distribution of wheel contact points and (b) distribution of rail contact points, (c) vertical wheel-rail force, (d) lateral wheel-rail force, (e) derailment coefficient and (f) wheel lift.

Based on the simulation results, the risk of wheel climb derailment increases with the decrease of running speed at low speed range when the empty wagon passing straight through a turnout.

6. Conclusions

This paper presented a study on the dynamic derailment of an empty wagon passing straight through a turnout. The potential factors that inducing train derailment in turnout area were analyzed firstly based on the field investigation. A dynamic model for the wagon-turnout interaction was established. By means of simulation, the characteristics of wheel-rail interaction in turnout area were investigated, and the key influencing factors related to the derailment of train wagons in turnout were discussed. The following conclusions are drawn from this study:

(1) For an empty wagon passing straight through a turnout, the growing inclined surface of switch rail, the harmful space of frog, the condition of wheel-rail interface, the lateral coupler force as well as the train speed are recognized to be key factors to derailment.

(2) The coupler force promotes the risk of wheel climb derailment in turnout area significantly under the condition of a large coupler yaw angle. The large lateral component of the coupler force makes the wheel climb the switch rail. The larger the

coupler force is applied, the earlier the wheel climb derailment happens. The possibility of wheel climb derailment can be reduced by decreasing coupler force.

(3) Wheel-rail friction coefficient has a great influence on the possibility of wheel climb derailment in turnout area. A small wheel-rail friction coefficient can effectively prevent the wheel climb when the flange contacts with the rail. The rail lubrication could be an effective measurement for preventing wheel climb in turnout area.

(4) At low-speed range, the risk of wheel climb derailment increases with the decrease of running speed when the empty wagon passing straight through a turnout, and the large braking force should be avoided.

It should be noted that the employed turnout in this study is a perfect turnout without any abrasions. In actual conditions, the rail wear in turnout area is extremely serious, especially in heavy-haul line. The running safety of vehicles in turnout area considering the complicated wheel/rail wear conditions is worthy of further studies.

Acknowledgements

The authors would like to thank the State Key Laboratory of Traction Power for providing equipment and materials to this project, and the China Dazhun Railway Company for the cooperation and support. The authors are also grateful to the reviewers for valuable technical advice and help in improving the text of this paper.

Disclosure statement

No potential conflict of interest was reported by the authors.

Funding

The authors are grateful for the financial support provided by the National Natural Science Foundation of China (Grant No. 51825504 and 51735012) and the Program of Introducing Talents of Discipline to Universities (111 Project) (Grant No. B16041).

References

[1] Wu H, Wilson N. Railway vehicle derailment and prevention. In: Iwnicki S, editor. Handbook of railway vehicle dynamics. London: Taylor & Francis; 2006. p. 209–238.

[2] Dindar S, Kaewunruen S. Assessment of Turnout-Related Derailments by Various Causes. International Congress and Exhibition 'Sustainable Civil Infrastructures: Innovative Infrastructure Geotechnology'. Springer, Cham, 2017: 27-39.

[3] Nadal, MJ. Locomotives a Vapeur, Collection Encyclopedie Scientifique, Biblioteque de Mecanique Appliquee et Genie, Vol. 186, Paris, 1908.

[4] Weinstock, H. Wheel climb derailment criteria for evaluation of rail vehicle safety, Proceedings of ASME Winter Annual Meeting, 84-WA/RT-1, New Orleans, LA, 1984.

[5] Matsudaira, T. Dynamics of High Speed Rolling Stock, Japanese National Railways RTRI Quarterly Reports, Special Issue, 1963.

[6] Koci HH, Swenson CA. Locomotive Wheel-Loading — A System Approach, General Motors Electromotive Division, LaGrange, IL, February, 1978.

[7] M1001, AAR Mechanical Division, Manual of Standards and Recommended Practices, Section C —Part II, Volume 1, Chapter XI, Section 11.5.2 Track-Worthiness Criteria, Adopted 1987, Revised 1993.

[8] Federal Railroad Administration. Track Safety Standards, Part 213, Subpart G, September, 1998.

[9] Zhai W. Vehicle-Track Coupled Dynamics: Theory and Applications. Singapore: Springer; 2019.

[10] Zhai W, Chen G. Method and criteria for evaluation of wheel derailment based on wheel vertical rise. Journal of the China Railway Society. 2001;23(2):17–26. (In Chinese)

[11] Zeng Q, Xiang J, Zhou Z. Analysis Theory of Train Derailment and Its Application.

Changsha: Central South University Press; 2006. (In Chinese)

[12] Xiang J, Zeng Q. A study on mechanical mechanism of train derailment and preventive measures for derailment. Veh Syst Dyn. 2005; 43(2):121-147.

[13] Barbosa RS. A 3D contact force safety criterion for flange climb derailment of a railway wheel. Veh Syst Dyn. 2004;42(5):289-300.

[14] Zeng J, Wu P. Study on the wheel/rail interaction and derailment safety. Wear. 2008; 265(9-10):1452-1459.

[15] Zeng J, Guan QH. Study on flange climb derailment criteria of a railway wheelset. Veh Syst Dyn. 2008;46(3):239-251.

[16] Ling L, Dhanasekar M, Thambiratnam D P. Frontal collision of trains onto obliquely stuck road trucks at level crossings: derailment mechanisms and simulation. I J Impact Eng. 2017;100:154-165.

[17] DOI H, MIYAMOTO T, SUZUMURA J, et al. Change in Surface Condition of Turned Wheel and Effectiveness of Lubrication against Flange Climb Derailment. Quarterly Report of RTRI, 2012;53(2):70-76.

[18] Xu J, Wang J, Wang P, et al. Study on the derailment behaviour of a railway wheelset with solid axles in a railway turnout. Veh Syst Dyn. 2020;58(1):123-143.

[19] Xu J, Wang P, Wang L, et al. Effects of profile wear on wheel–rail contact conditions and dynamic interaction of vehicle and turnout. Adv Mech Eng. 2016;8(1): 1-8.

[20] Sun YQ, Cole C, McClanachan M. The calculation of wheel impact force due to the interaction between vehicle and a turnout. Proc Inst Mech Eng F J Rail Rapid Transit. 2010;224(5):391-403.

[21] Dos Santos GFM, Barbosa RS. Modeling of a railway vehicle travelling through a turnout. Proc Inst Mech Eng F J Rail Rapid Transit. 2016;230(4):1397-1404.

[22] Ren Z, Sun S, Xie G. A method to determine the two-point contact zone and transfer of wheel–rail forces in a turnout. Veh Syst Dyn. 2010;48(10):1115-1133.

[23] Ren Z S, Sun S, Zhai W. Study on lateral dynamic characteristics of vehicle/turnout system. Veh Syst Dyn. 2005;43(4):285-303.

[24] Kassa E, Nielsen JCO. Dynamic interaction between train and railway turnout: full-scale field test and validation of simulation models. Veh Syst Dyn. 2008;46(S1):521-534.

[25] Ge X, Wang K, Guo L, et al. Investigation on Derailment of Empty Wagons of Long Freight Train during Dynamic Braking. Shock and Vibration, 2018.

[26] Wang K, Zhang R, Chen Z, et al. Effect of coupler position errors on dynamic performance of heavy haul locomotive. J. Southwest Jiaotong Univ. 2016;50(6):1041–1046. (In Chinese)

[27] Shi Z, Wang K, Guo L, et al. Effect of arc surfaces friction coefficient on coupler stability in heavy haul locomotives: simulation and experiment. Veh Syst Dyn. 2017;55(9):1368-1383.

[28] Lv K, Wang K, Chen Z, et al. The effect of the secondary lateral stopper on the compressed stability of the couplers and running safety of the locomotives. Proc Inst Mech Eng F J Rail Rapid Transit. 2018;232(3):851-862.

[29] Guo L, Wang K, Chen Z, et al. Analysis of the car body stability performance after coupler jack-knifing during braking. Veh Syst Dyn. 2018;56(6):900-922.

[30] Wu Q, Spiryagin M, Cole C. Advanced dynamic modelling for friction draft gears. Veh Syst Dyn. 2015;53(4):475-492.

[31] Liu P, Zhai W, Wang K. Establishment and verification of three-dimensional dynamic model for heavy-haul train–track coupled system. Veh Syst Dyn. 2016;54(11):1511-1537.

[32] Kalker JJ. Three-dimensional elastic bodies in rolling contact. Vol. 2. Dordrecht: Springer Science & Business Media; 1990.

[33] Kalker JJ. A fast algorithm for the simplified theory of rolling contact. Veh Syst Dyn. 1982;11(1): 1-13.

[34] Xiao Q, Wang C, Zhou X, et al. Analysis on the characteristics of wheel/rail rolling contact under different friction coefficient. China Railw. Sci. 2011;32(4):66-71. (In Chinese)